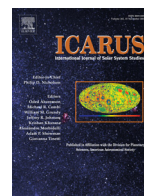




ELSEVIER

Contents lists available at ScienceDirect

Icarus

journal homepage: www.elsevier.com/locate/icarus

New constraints on Saturn's interior from Cassini astrometric data

Valéry Lainey^{a,*}, Robert A. Jacobson^b, Radwan Tajeddine^{c,a}, Nicholas J. Cooper^{d,a}, Carl Murray^d, Vincent Robert^{e,a}, Gabriel Tobie^f, Tristan Guillot^g, Stéphane Mathis^h, Françoise Remus^{i,a,h}, Josselin Desmars^{j,a}, Jean-Eudes Arlot^a, Jean-Pierre De Cuyper^k, Véronique Dehant^k, Dan Pascu^l, William Thuillot^a, Christophe Le Poncin-Lafitte^m, Jean-Paul Zahn^l

^aIMCCE, Observatoire de Paris, PSL Research University, CNRS, Sorbonne Universités, UPMC Univ. Paris 06, Univ. Lille, France

^bJet Propulsion Laboratory, California Institute of Technology, 4800 Oak Grove Drive, Pasadena, CA 91109-8099, United States

^cCenter for Astrophysics and Planetary Science, Cornell University, Ithaca, NY 14853, USA

^dQueen Mary University of London, Mile End Rd, London E1 4NS, United Kingdom

^eIPSA, 7-9 rue Maurice Grandcoing, 94200 Ivry-sur-Seine, France

^fLaboratoire de Planétologie et Géodynamique de Nantes, Université de Nantes, CNRS, UMR 6112, 2 rue de la Houssinière, 44322 Nantes Cedex 3, France

^gLaboratoire Lagrange, CNRS UMR 7293, Université de Nice-Sophia Antipolis, Observatoire de la Côte d'Azur, B.P. 4229, 06304 Nice Cedex 4, France

^hLaboratoire AIM Paris-Saclay, CEA/DRF - Université Paris Diderot - CNRS, IRFU/SAP Centre de Saclay, 91191 Gif-sur-Yvette, France

ⁱLUTH-Observatoire de Paris, UMR 8102 du CNRS, 5 place Jules Janssen, 92195 Meudon Cedex, France

^jObservatório Nacional, Rua José Cristino 77, São Cristóvão, Rio de Janeiro CEP 20.921-400, Brazil

^kRoyal Observatory of Belgium, Avenue Circulaire 3, 1180 Uccle, Bruxelles, Belgium

^lUSNO, 3450 Massachusetts Avenue Northwest, Washington, DC 20392, United States

^mSYRTE, Observatoire de Paris, PSL Research University, CNRS, Sorbonne Universités, UPMC Univ. Paris 06, LNE, 61 avenue de l'Observatoire, 75014 Paris, France

ARTICLE INFO

Article history:

Received 4 October 2015

Revised 8 July 2016

Accepted 24 July 2016

Available online xxx

Keywords:

Astrometry

Interior

Saturn

ABSTRACT

Using astrometric observations spanning more than a century and including a large set of Cassini data, we determine Saturn's tidal parameters through their current effects on the orbits of the eight main and four coorbital Moons. We have used the latter to make the first determination of Saturn's Love number from observations, $k_2=0.390 \pm 0.024$, a value larger than the commonly used theoretical value of 0.341 (Gavrilov & Zharkov, 1977), but compatible with more recent models (Helled & Guillot, 2013) for which the static k_2 ranges from 0.355 to 0.382. Depending on the assumed spin for Saturn's interior, the new constraint can lead to a significant reduction in the number of potential models, offering great opportunities to probe the planet's interior. In addition, significant tidal dissipation within Saturn is confirmed (Lainey et al., 2012) corresponding to a high present-day tidal ratio $k_2/Q=(1.59 \pm 0.74) \times 10^{-4}$ and implying fast orbital expansions of the Moons. This high dissipation, with no obvious variations for tidal frequencies corresponding to those of Enceladus and Dione, may be explained by viscous friction in a solid core, implying a core viscosity typically ranging between 10^{14} and 10^{16} Pa.s (Remus et al., 2012). However, a dissipation increase by one order of magnitude at Rhea's frequency could suggest the existence of an additional, frequency-dependent, dissipation process, possibly from turbulent friction acting on tidal waves in the fluid envelope of Saturn (Ogilvie & Lin, 2004; Fuller et al. 2016).

© 2016 Elsevier Inc. All rights reserved.

1. Introduction

Tidal effects among planetary systems are the main driver in the orbital migration of natural satellites. They result from physical processes arising in the interior of celestial bodies, not observable necessarily from surface imaging. Hence, monitoring the Moons'

motions offers a unique opportunity to probe the interior properties of a planet and its satellites. In common with the martian and jovian systems (Lainey et al., 2007, 2009), the orbital evolution of the saturnian system due to tidal dissipation can be derived from astrometric observations of the satellites over an extended time period. In that respect, the presence of the Cassini spacecraft in orbit around Saturn since 2004 has provided unprecedented astrometric and radio-science data for this system with exquisite precision. These data open the door for estimating a potentially large

* Corresponding author.

E-mail address: lainey@imcce.fr (V. Lainey).

number of physical parameters simultaneously, such as the gravity field of the whole system and even separating the usually strongly correlated tidal parameters k_2 and Q .

The present work is based on two fully independent analyses (modeling, data, fitting procedure) performed at IMCCE and JPL, respectively. Methods are briefly described in Section 2. Section 3 provides a comparison between both analyses as well as a global solution for the tidal parameters k_2 and Q of Saturn. Section 4 describes possible interior models of Saturn compatible with our observations. Section 5 discusses possible implications associated with the strong tidal dissipation we determined.

2. Material and methods

Both analyses stand on numerical computation of the Moons' orbital states at any time, as well as computation of the derivatives of these state vectors (see Section 2.1) with respect to: (i) their initial state for some reference epoch; (ii) many physical parameters. Tidal effects between both the Moons and the planet are introduced by means of the amplitude of the tidal bulge and its time lag associated to dissipation processes. The gravitational effect of the tidal bulge is classically described by the tidal Love number k_2 and the tidal ratio k_2/Q . The Love number k_2 is defined as the ratio between the gravitational potential induced by the tidally-induced mass redistribution and the tide-generating potential. As the interior does not respond perfectly to the tidal perturbations, because of internal friction applied on tides, there is a time lag between the tide-raising potential and the tidally-induced potential. The torque created by this lag is proportional to the so-called tidal ratio k_2/Q . The amplitude and lag of the tide potential can also be described using a complex representation of the Love number, where the real part correspond to the part of the potential aligned with the tide-raising potential, while the imaginary part describes the dissipative part (see also Section 4). The factor Q , often called the quality factor (Kaula 1964), or the specific dissipation function, Q^{-1} , in its inverse form, is inversely proportional to the amount of energy dissipated by tidal friction in the deformed object. Coupled tidal effects such as tidal bulges raised on Saturn by one Moon and acting on another are considered. Besides the eight main Moons of Saturn, the coorbital Moons Calypso, Telesto, Polydeuces, and Helene are integrated in both studies.

Although the two tidal parameters k_2 and Q often appear independently in the equations of motion, the major dynamical effect by far is obtained when the tide raised by a Moon on its primary acts back on this same Moon. In this case, only the ratio k_2/Q is present as a factor for the major term, therefore preventing an independent fit of k_2 and Q . However, the small co-orbital satellites raise negligible tides on Saturn and yet react to the tides raised on the planet by their parent satellites (see Figure in Appendix A.1). This unique property allows us to make a fit for k_2 that is almost independent of Q (see Appendix A.1). In particular, we find that the modeling of such cross effects between the coorbital moons allows us to obtain a linear correlation between k_2 and Q of only 0.03 (Section 3 and Appendix A.4). Thanks to the inclusion of Telesto, Calypso, Helene and Polydeuces, we can estimate k_2 essentially around the tidal frequencies of Tethys and Dione.

2.1. IMCCE's approach

The IMCCE approach benefits from the NOE numerical code that was successfully applied to the Mars, Jupiter, and Uranus systems (Lainey et al., 2007, 2008, 2009). It is a gravitational N-body code that incorporates highly sensitive modeling and can generate partial derivatives needed to fit initial positions, velocities, and other parameters (like the ratio k_2/Q) to the observational data. The code includes (i) gravitational interaction up to degree two in

the spherical harmonics expansion of the gravitational potential for the satellites and up to degree 6 for Saturn (Jacobson et al. 2006); (ii) the perturbations of the Sun (including inner planets and the Moon by introducing their mass in the Solar one) and Jupiter using DE430 ephemerides; (iii) the Saturnian precession; (iv) the tidal effects introduced by means of the Love number k_2 and the quality factor Q .

The dynamical equations are numerically integrated in a Saturncentric frame with inertial axes (conveniently the Earth mean equator J2000). The equation of motion for a satellite P_i can be expressed as (Lainey et al. 2007)

$$\ddot{\vec{r}}_i = -\frac{G(m_0 + m_i)\vec{r}_i}{r_i^3} + \sum_{j=1, j \neq i}^N Gm_j \left(\frac{\vec{r}_j - \vec{r}_i}{r_{ij}^3} - \frac{\vec{r}_j}{r_j^3} \right) + G(m_0 + m_i)\nabla_i U_{i0} + \sum_{j=1, j \neq i}^N Gm_j \nabla_j U_{j0} + \frac{(m_0 + m_i)}{m_i m_0} (\vec{F}_{i0}^T - \vec{F}_{0i}^T) - \frac{1}{m_0} \sum_{j=1, j \neq i}^N (\vec{F}_{j0}^T - \vec{F}_{0j}^T) + GR \quad (1)$$

Here, \vec{r}_i and \vec{r}_j are the position vectors of the satellite P_i and a body P_j (another satellite, the Sun, or Jupiter) with mass m_j , subscript 0 denotes Saturn, U_{ij}^T is the oblateness gravity field of body P_i at the position of body P_k , GR are corrections due to General Relativity (Newhall et al. 1983) and \vec{F}_{ik}^T the force received by P_i from the tides it raises on P_k . This force is equal to (Lainey et al. 2007)

$$\vec{F}_{ik}^T = -\frac{3k_2 Gm_i^2 R^5 \Delta t}{r_{kl}^8} \left(\frac{2\vec{r}_{kl}(\vec{r}_{kl} \cdot \vec{v}_{kl})}{r_{kl}^2} + (\vec{r}_{kl} \times \vec{\Omega} + \vec{v}_{kl}) \right) \quad (2)$$

where $\vec{r}_{kl} = \vec{r}_k - \vec{r}_l$, $\vec{v}_{kl} = d\vec{r}_{kl}/dt$, $\vec{\Omega}$, R , and Δt being the instantaneous rotation vector, equatorial radius and time potential lag of P_k , respectively. The time lag Δt is defined by

$$\Delta t = \text{Tarctan}(1/Q)/2\pi \quad (3)$$

where T is the period of the main tidal excitation. For the tides raised on Enceladus, T is equal to $2\pi/n$ (n being Enceladus' mean motion) as we only considered the tide raised by Saturn. For Saturn's tidal dissipation, T is equal to $2\pi/2(\Omega - n_i)$ where Ω is the spin frequency of Saturn and n_i is the mean motion of the tide raising saturnian Moon P_i . Δt depends on the tidal frequency and on Q , therefore it is not a constant parameter.

It is clear from the second term in the right hand side of Eqs. (2) and (3) that k_2 and Q are completely correlated. To separate both parameters, we consider the action on any Moon of the tides raised on Saturn by all other Moons (see also Appendix A.1). Neglecting tidal dissipation in that case provides the extra terms

$$\sum_{j=1, j \neq i}^N \frac{\vec{F}_{ij}^T}{m_i} = \frac{3k_2 Gm_j R^5}{2r_j^5 r_i^5} \left[-\frac{5(\vec{r}_i \cdot \vec{r}_j)^2 \vec{r}_i}{r_i^2} + r_j^2 \vec{r}_i + 2(\vec{r}_i \cdot \vec{r}_j) \vec{r}_j \right]. \quad (4)$$

For an unspecified parameter c_i of the model that shall be fitted (e.g. $\vec{r}(t_0)$, $d\vec{r}/dt(t_0)$, Q ...), a useful relation is (Lainey et al. 2012 and references therein)

$$\frac{\partial}{\partial c_i} \left(\frac{d^2 \vec{r}_i}{dt^2} \right) = \frac{1}{m_i} \left[\sum_j \left(\frac{\partial \vec{F}_i}{\partial \vec{r}_j} \frac{\partial \vec{r}_j}{\partial c_i} + \frac{\partial \vec{F}_i}{\partial \vec{r}_j} \frac{\partial \dot{\vec{r}}_j}{\partial c_i} \right) + \frac{\partial \vec{F}_i}{\partial c_i} \right], \quad (5)$$

where \vec{F}_i is the right hand side of Eq. (1) multiplied by m_i . Partial derivatives of the solutions with respect to initial positions and velocities of the satellites and dynamical parameters are computed from simultaneous integration of Eqs. (5) and (1).

Here, fourteen Moons of Saturn are considered all together, i.e. the eight main Moons and six coorbital Moons (Epimetheus, Janus, Calypso, Telesto, Helene, and Polydeuces). All the astrometric observations already considered in Lainey et al. (2012) and Desmars et al. (2009) are used, with the addition of a large set of ISS-Cassini data (Tajeddine et al., 2013, 2015; Cooper et al. 2014). We also include a new reduction of old photographic plates, obtained at USNO between the years 1974 and 1998. As part of the ESPaCE European project, the scanning and new astrometric reduction of these plates were performed recently at Royal Observatory of Belgium and IMCCE, respectively (Robert et al. 2011, 2016). We use a weighted least squares inversion procedure and minimize the squared differences between the observed and computed positions of the satellites in order to determine the parameters of the model. For each fit, the following parameters are released simultaneously and without constraints: the initial state vector and mass of each Moon, the mass, the gravitational harmonic J_2 , the orientation and the precession of the pole of Saturn as well as its tidal parameters k_2 and Q . Tidal dissipation within the Moons is neglected, except in Enceladus for which strong tides are believed to take place. No da/dt term is released for Mimas. In particular, it appears that the large signal obtained in Lainey et al. (2012) can be removed after fitting the gravity field of the Saturn system. Indeed, due to its long period libration (about 70 years), the 2:1 Mimas-Tethys resonance strongly affects the dynamical evolution of Mimas' orbit over the considered time span of observations. Due to exchange of angular momentum between the rings and Mimas, a quadratic effect on Mimas' longitude may be strongly correlated with the libration amplitude. Since the libration is conditioned by the mass of Mimas and Tethys, Lainey et al. (2012) fixed their value to former estimates that benefited from the first Cassini data (Jacobson 2006) to solve for da/dt . Unfortunately, even a small error on the mass of the two Moons was sufficient to generate erroneous behavior in the libration angle, strongly affecting the da/dt determination. In this work, and thanks to Cassini data, the mass of Saturn and all main Moons are fitted accurately.

2.2. JPL's approach

The second approach incorporates the tidal parameters into the ongoing determination of the satellite ephemerides and Saturnian system gravity parameters that support navigation for the Cassini Mission. Initial results from that work appear in Jacobson et al. (2006). For Cassini the satellite system is restricted to the eight major satellites, Phoebe, and the lagrangians Helene, Telesto, and Calypso. The analysis procedure is to repeat all of the Cassini navigation reconstructions but with a common set of ephemerides and gravity parameters. We combine these new reconstructions with other non-Cassini data sets to obtain the updated ephemerides and revised gravity parameters. The non-Cassini data include radiometric tracking of the Pioneer and Voyager spacecraft, imaging from Voyager, Earth-based and HST astrometry, satellite mutual events (eclipses and occultations), and Saturn ring occultations. We process the data via a weighted least-squares fit that adjusts our models of the orbits of the satellites and the four spacecraft (Pioneer, Voyager 1, Voyager 2, Cassini). Peters (1981) and Moyer (2000) describe the orbital models for the satellites and spacecraft, respectively. The set of gravity related parameters adjusted in the fit contains the GMs of the Saturnian system and the satellites (Helene, Telesto, and Calypso are assumed massless), the gravitational harmonics of Saturn, Enceladus, Dione, Rhea, and Titan, Saturn's polar moment of inertia, the orientation of Saturn's pole, and the tidal parameters k_2 and Q .

3. Results

Since tidal effects within Saturn and Enceladus have almost opposite orbital consequences, Lainey et al. (2012) could not solve for the Enceladus tidal ratio k_2^E/Q^E . Here, we face a similar strong correlation and follow their approach by considering two extreme scenarios for Enceladus' tidal state. In a first inversion, we neglect dissipation in Enceladus and obtain for Saturn k_2 , $k_2^{(I)}=0.371 \pm 0.003$, $k_2^{(J)}=0.381 \pm 0.011$ (formal error bar, 1σ) where the indices I and J refer to the IMCCE and JPL solutions, respectively. The Saturn tidal ratio that we obtain is $k_2/Q^{(I)}=(1.32 \pm 0.25) \times 10^{-4}$, $k_2/Q^{(J)}=(1.04 \pm 0.19) \times 10^{-4}$. In a second inversion, we assume Enceladus to be in a state of tidal equilibrium (Meyer & Wisdom, 2007), obtaining $k_2^{(I)}=0.372 \pm 0.003$, $k_2^{(J)}=0.402 \pm 0.011$ and $k_2/Q^{(I)}=(2.07 \pm 0.26) \times 10^{-4}$, $k_2/Q^{(J)}=(1.22 \pm 0.23) \times 10^{-4}$. If both studies are generally in good agreement within the uncertainty of the measurements (see also Tables 1 and 2), the last $k_2/Q^{(I)}$ value stands at 3σ of the JPL estimation. This possibly reflects the difference in the data sets, since JPL introduced radio-science data, while IMCCE introduced scanning data. Nevertheless, both estimates suggest strong tidal dissipation, at least about five times larger than previous theoretical estimates (Sinclair, 1983). Merging IMCCE's and JPL's results into one value by overlapping the extreme 1σ values, we get $k_2=0.390 \pm 0.024$ and $k_2/Q=(1.59 \pm 0.74) \times 10^{-4}$. These last error bars are not formal 1σ values anymore, but the likely interval of expected physical values.

Last, to assess a possibly large variation in Saturn's Q as function of tidal frequency, we followed Lainey et al. (2012) and released as free parameters four different Saturnian tidal ratios k_2/Q associated with the Enceladus', Tethys', Dione's, and Rhea's tides (see Tables 1 and 2). It turns out that no significant change for the k_2 estimation arises with an overall result of $k_2=0.390 \pm 0.024$. Moreover, global solutions for k_2/Q ratios are equal to $(20.70 \pm 19.91) \times 10^{-5}$, $(15.84 \pm 12.26) \times 10^{-5}$, $(16.02 \pm 12.72) \times 10^{-5}$, $(123.94 \pm 17.27) \times 10^{-5}$ at Enceladus', Tethys', Dione's and Rhea's tidal frequency, respectively. Increasing the number of frequencies to be tested may be problematic. If the tidal bulges raised by Titan on Saturn are much larger than those raised by the other Moons, their feedback on Titan's orbit is significantly smaller. This can easily be checked from analytical expression of orbital expansion of Moons raising tides on their primary (Kaula 1964). As a consequence, we did not release Saturn's k_2/Q at Titan's tidal frequency. Moreover, since Mimas and Tethys are locked in a mean motion resonance, they share their orbital energy and angular momentum. Hence, the action of tides raised on Saturn by Mimas and Tethys is distributed among the resonant pair. In the limit of our current measurements, this prevented solving simultaneously for Saturn's k_2/Q at Mimas and Tethys frequencies. Hence, Saturn's k_2/Q was kept fixed at its former constant estimation (see above) for Mimas as well as for all other Moons, with the exception of Enceladus, Tethys, Dione and Rhea. We provide in Fig. 1 a plot showing all global k_2/Q ratios associated with constant and non-constant assumptions.

4. Modeling Saturn's interior

To model the tidal response of Saturn's interior and to compare it to the k_2 and k_2/Q values inferred in the present study, we consider a wide range of interior models consistent with the gravitational coefficients measured using the Cassini spacecraft (Helled & Guillot 2013). In total, 302 interior models, corresponding to various core size and composition, helium phase separation and enrichment in heavy elements in the external envelope, have been tested. Each interior model is characterized by radial profiles of density, ρ , and bulk modulus, K .

Table 1
Fitting k_2 and variable Saturnian Q at Enceladus (S2), Tethys (S3), Dione (S4) and Rhea (S5) frequencies.

	k_2	k_2/Q (S2)	k_2/Q (S3)	k_2/Q (S4)	k_2/Q (S5)
IMCCE	0.372 \pm 0.003	(7.4 \pm 3.1) $\times 10^{-5}$	(10.9 \pm 6.1) $\times 10^{-5}$	(16.1 \pm 3.8) $\times 10^{-5}$	(122.3 \pm 15.0) $\times 10^{-5}$
JPL	0.377 \pm 0.011	(5.5 \pm 4.7) $\times 10^{-5}$	(6.0 \pm 2.4) $\times 10^{-5}$	(21.5 \pm 7.3) $\times 10^{-5}$	(125.8 \pm 14.9) $\times 10^{-5}$

Table 2
Fitting k_2 and variable Saturnian Q at Enceladus (S2), Tethys (S3), Dione (S4) and Rhea (S5) frequencies assuming Enceladus' tidal equilibrium.

	k_2	k_2/Q (S2)	k_2/Q (S3)	k_2/Q (S4)	k_2/Q (S5)
IMCCE	0.372 \pm 0.003	(18.1 \pm 3.1) $\times 10^{-5}$	(11.9 \pm 6.1) $\times 10^{-5}$	(15.0 \pm 3.8) $\times 10^{-5}$	(121.6 \pm 15.0) $\times 10^{-5}$
JPL	0.394 \pm 0.011	(27.1 \pm 13.5) $\times 10^{-5}$	(21.5 \pm 6.6) $\times 10^{-5}$	(5.4 \pm 2.1) $\times 10^{-5}$	(127.9 \pm 13.3) $\times 10^{-5}$

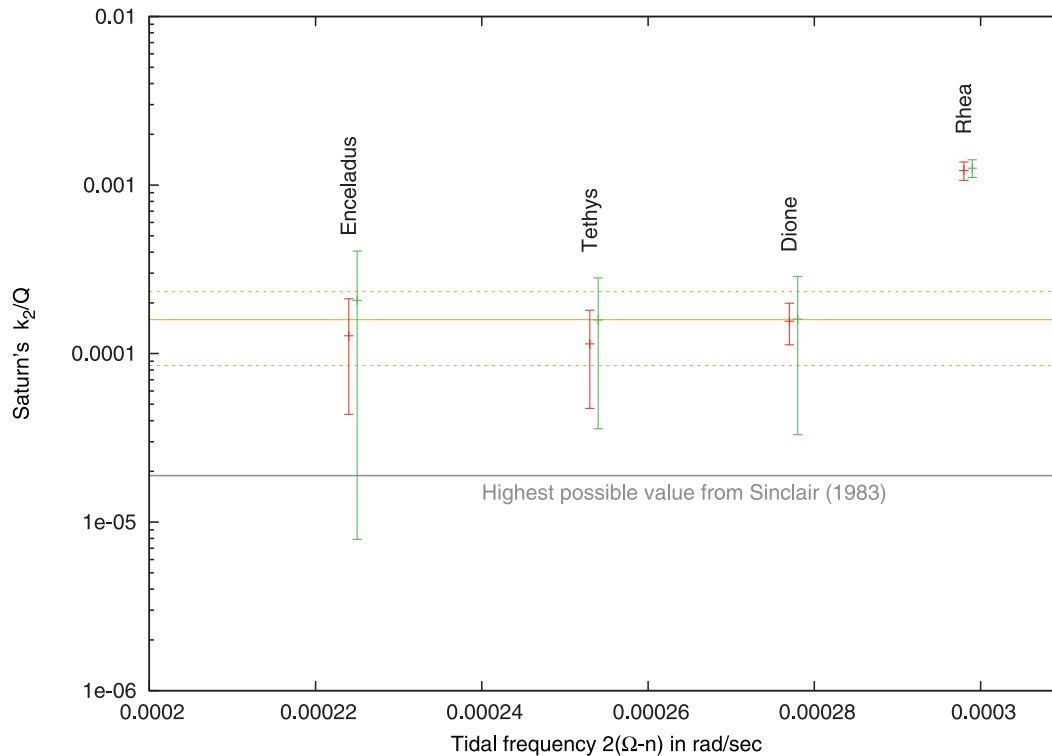


Fig. 1. Variation of the Saturnian tidal ratio k_2/Q as a function of tidal frequency $2(\Omega-n)$, where Ω and n denote its rotation rate and the Moon's mean motion, respectively. Four frequencies are presented associated with Enceladus', Tethys', Dione's and Rhea's tides. IMCCE and JPL solutions are in red and green, respectively. They are shown slightly shifted from each other along the X-axis for better visibility. Orange lines refer to the global estimation $k_2/Q=(15.9 \pm 7.4) \times 10^{-5}$. (For interpretation of the references to color in this figure legend, the reader is referred to the web version of this article).

In giant planets, two main mechanisms are invoked for tidal dissipation: the viscous dissipation associated to viscoelastic deformation of a solid core (as initially proposed by Dermott (1979) and further explored here) and the fluid friction applied on tidal waves propagating in the deep gaseous envelope (see e.g. Ogilvie & Lin 2004 and the discussion hereafter). As demonstrated in Guenel, Mathis and Remus (2014), these two mechanisms may have comparable strengths and superpose.

Here, the tidal response of Saturn's interior is first computed from all the considered density profiles assuming that the core is solid and viscoelastic, with radius R_{core} (varying typically between 7000 and 16,000 km) overlaid by a thick non-dissipative fluid envelope (to explore the own effect of the core), similar to the approach of Remus et al. (2012, 2015). The envelope is only taken into account for the hydrostatic effects it applies on the core. The complex Love number k_2^c (including both the response aligned with tide-raising potential and the dissipative part in quadrature) is computed by integrating the 5 radial functions, y_i , describing the displacements, stresses, and gravitational potential from the planet

center to the surface, following the formalism initially introduced by Alterman et al. (1959). The viscoelastic deformation in the solid viscoelastic core is computed using the compressible elastic formulation of Takeuchi & Saito (1972), adapted to viscoelastic media (see Tobie et al., 2005 for more details). For the fluid envelope, the static formulation of Saito (1974) is used. In this formalism, the fluid friction is not modeled. However, it allows us to take into account the gravitational effects of the fluid envelope on the solid core deformation, which has a strong impact in the case of very thick fluid envelope like in the case of Saturn as demonstrated by Dermott (1979) and Remus et al. (2012, 2015). The system of differential equations (6 in the core and 2 in the envelope) is solved by integrating from the center to the surface three independent solutions using a fifth order Runge-Kutta method with adaptive stepsize control, and by applying the appropriate condition at the solid core/fluid envelope interface and at the surface (see Takeuchi & Saito 1972 and Tobie et al. 2005 for more details). The complex Love number k_2^c is determined from the complex 5th radial function at the planet surface, $y_5^c(R_s)$, and the global dissipation

function by the ratio between the imaginary part and the modulus of k_2^c : $k_2 = |k_2^c| = |y_5^c(R_s) - 1|$; $Q^{-1} = -\text{Im}(k_2^c)/|k_2^c|$.

For the solid core, a compressible Maxwell rheology, characterized by the bulk modulus K , the shear modulus μ , and the viscosity η , is assumed. As the mechanical properties of such a core are totally unknown, a wide range of parameter values is considered. As we will show hereafter, the Q factor of Saturn can be explained only for a limited range of viscoelastic parameters, thus providing useful constraints on Saturn's core structure and rheology. The shear modulus is determined from the bulk modulus assuming a constant μ/K ratio varying between 0.001 and 1, and the viscosity is assumed constant over a range varying between 10^{12} and 10^{18} Pa.s. For comparison, the μ/K ratio in the inner core of the Earth is about 0.12 (Dziewonski and Anderson, 1981), and its viscosity is estimated typically between 10^{14} and 10^{20} Pa.s (Karato, 2008). Obviously, Saturn's core is different from Earth's metallic inner core due to difference in pressure and composition. However, this comparison gives us an estimate of the typical parameter values we might expect in Saturn.

In order to test the validity of our numerical code, we compared our numerical solutions with the analytical solutions derived by Remus et al. (2012) for a viscoelastic core and a fluid envelope with constant density. As illustrated on Fig. A.2, we reproduce almost perfectly the analytical value of the tidal Love number. For the dissipation function, the agreement is also very good, the difference between the analytical and numerical solutions never exceed a few per cent. To further test our code, we also compared with the solution provided by Kramm et al. (2011) for a density distribution of a $n=1$ polytrope: we obtained $k_2=0.5239$, while the value reported by Kramm et al. (2011) is 0.5198, which corresponds to a difference of less than 0.8%.

Our calculations confirm that the real part of the tidal Love number (k_2) of the planet is almost entirely determined by the density profile; therefore it is a very close to the fluid Love number. For the 302 tested interiors models, corresponding to various core size and composition of the core and fluid envelope, we obtained values of k_2 ranging between 0.355 and 0.381. The lowest values are obtained for fast deep rotation (10h32') and high-density core (modeled with the EOS of pure rock), while the highest values correspond to slow deep rotation (10h39') and low-density core (modeled with the EOS of pure ice). All tested models are consistent with the equatorial radius and the gravitational coefficients (J_2 , J_4 and J_6) determined by Cassini, within error bars. Although we did not test all possible models, based on these results, we can reasonably conclude that a k_2 value as high as 0.39 is incompatible with the observed gravitational coefficient. For slow rotation cases, all models with a low density ice-rich core have a k_2 value above 0.366, the lower limit inferred from astrometric measurements, while only about half of the models with a high density core exceeds this value. For fast rotation cases, only four tested models exceed this limit: all of them have a low-density core and a helium separation occurring at 1 Mbar, in line with recent determinations of hydrogen-helium phase separation (Morales et al., 2009). Even if we can notice some tendencies as a function of core size (Fig. 2), the k_2 value is controlled by several other internal parameters (core composition, helium separation, enrichment in heavy elements in the external envelope), which precludes any simple interpretation of the measured k_2 value in term of internal structure. Tests performed for a wide range of mechanical parameters for the core show that they have only very minor effects on the k_2 value. Varying the μ/K ratio from 0.001 to 1 results in only 0.2% of variations on the amplitude of k_2 . Nevertheless, it strongly affects the imaginary part of k_2 , and hence the quality factor, Q .

As shown in Fig. 3a and b, the global Q factor depends on the assumed shear modulus (hence the μ/K ratio) and the viscosity in

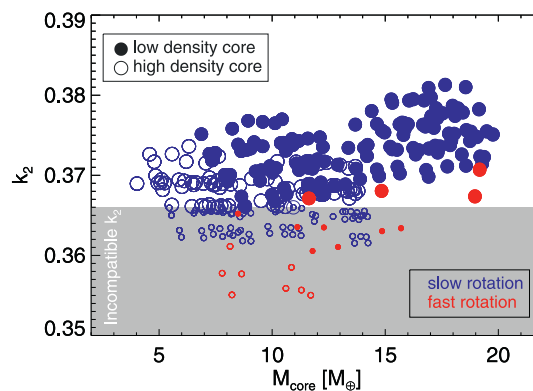


Fig. 2. Mass of the core and k_2 Love number for interior models of Saturn from Helled & Guillot (2013). Filled circles indicate models assuming a low density core (modeled using the equation of state of pure ice) while empty circles indicate models assuming a high density core (modeled using the EOS of rocks). Models in blue assume a “slow” deep rotation of 10h39m while models in red assume a “fast” deep rotation of 10h32m, more in line with the recent determination of Helled et al. (2015). The grey area indicates where values of k_2 are incompatible with our astrometric determination. (For interpretation of the references to color in this figure legend, the reader is referred to the web version of this article).

the core as well as on its size. The minimal values Q_{min} shown in Fig. 3a were obtained by systematically exploring the core viscosity for values comprised between 10^{12} and 10^{17} Pa.s. This shows that for $\mu/K \sim 0.1-0.5$, $Q < 3000$ can be obtained for core size comprised between 8000 and 17,000 km, with values as low as 200–300 for the largest core size (corresponding to ice-rich core). Fig. 3b shows the range of viscosity values for which Q remains below 3000. For models with ice core, $Q < 3000$ for viscosity values ranging between about 2.10^{13} and 2.10^{16} Pa.s. For small core radii ($< 11,000$ km) corresponding to a rock core, Q values lower than 3000 can also be found, but for a more restricted range of viscosity values, between typically 10^{15} and 10^{16} Pa.s. For a very low μ/K ratio (0.01), $Q < 3000$ can be obtained for large ice-rich cores and viscosity values of the order of 5.10^{13} – 5.10^{14} Pa.s. These possible ranges of viscosity are compatible with those derived previously in Remus et al. (2012, 2015) where simplified two-layer planetary models were used.

As illustrated in Fig. 4, the computed k_2/Q values vary only very weakly with tidal frequency, when compared to the frequency dependence expected for dissipation due to dissipation of tidal waves in the fluid envelope (e.g. Ogilvie & Lin, 2004). We obtained a weak frequency dependence with logarithmic rate of change with frequency ranging between -1 and $+1$, depending on the shear modulus and viscosity of the core. The slope, negative or positive, is determined by the Maxwell time, which is defined as the ratio between the viscosity and the shear modulus: $\tau = \eta/\mu$, relative to the forcing period. As in our models, the shear modulus vary as a function of radius in the core, the local Maxwell time vary as a function of radius. As an example, for $\mu/K=0.1$ and a viscosity value of 10^{15} – 10^{16} Pa.s, the Maxwell time typically varies between 0.9-9 hours at the center of the core to 0.2-2 hours at the core surface, while the tidal period varies between 6 and 8 h. As a consequence, for $\eta=10^{15}$ Pa.s, the slope is negative, while it is positive for $\eta=10^{16}$ Pa.s. In both cases, the weak frequency dependence is compatible with the tendencies inferred from astrometric observations for Enceladus, Tethys and Dione frequencies. Remarkably, for this viscosity range, we can reproduce the typical value of the observed k_2/Q .

Even though Q values as low as 200 can be obtained for large cores and appropriate viscoelastic parameters, it is not possible to explain with viscoelastic dissipation, Q values of the order of a few thousands at Enceladus' tidal frequency and of a few hundred at Rhea's tidal frequency. Additional dissipation processes in the deep gaseous envelope are thus required to explain the high dissipa-

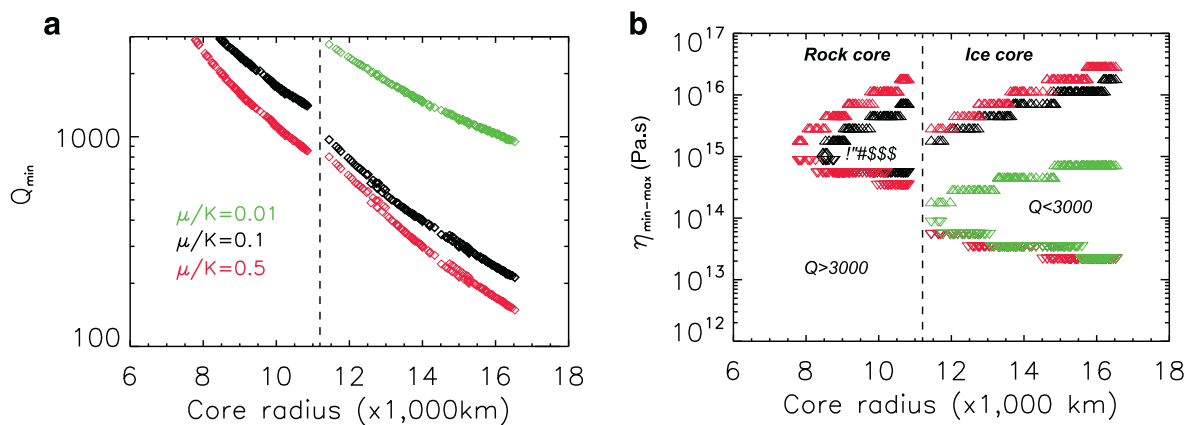


Fig. 3. (a) Minimum value of the quality factor, Q_{\min} , as a function of core radius for three different values of μ/K (0.01, 0.1, 0.5); (b) Range of viscosity values, $\eta_{\max}(\Delta)$ – $\eta_{\min}(\nabla)$, for which $Q < 3000$ for the three μ/K ratios displayed in (a). The dashed line indicates the transition between high density (rock-dominated) core and low density (ice-dominated) core. For this computation, the tidal frequency was fixed at $2.6 \times 10^{-4} \text{ rad.s}^{-1}$.

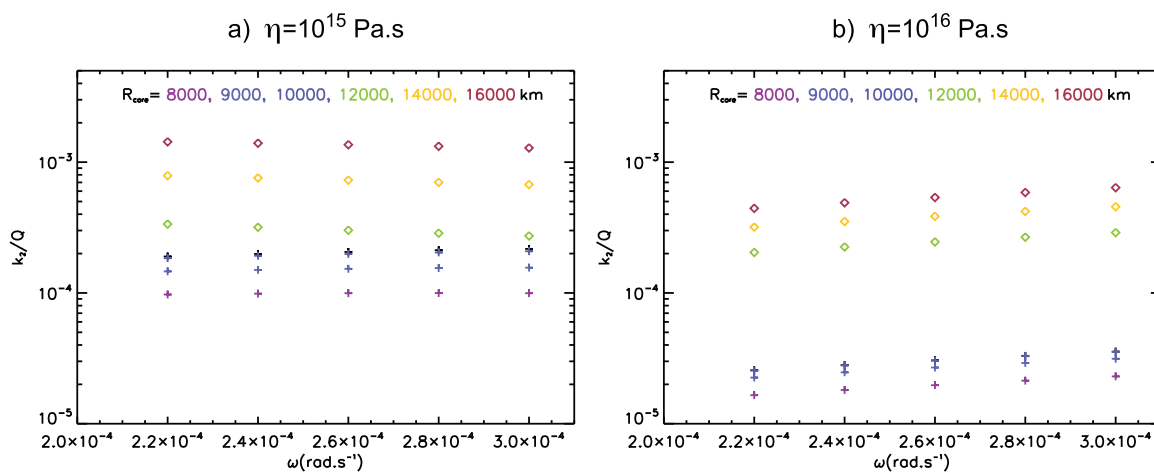


Fig. 4. k_2/Q values as a function of tidal frequency, ω , for two core viscosity values (10^{15} (a) and 10^{16} (b) Pa.s) for six different values of core radius. The μ/K ratio was fixed to 0.1 for these calculations.

tion inferred from observation at Rhea's tidal frequency. The best candidate is turbulent friction applied to tidal inertial waves (their restoring force is the Coriolis acceleration) in the deep, rapidly rotating, oblate convective envelope of Saturn that dissipates their kinetic energy (Ogilvie & Lin, 2004; Braviner & Ogilvie, 2015). This fluid dissipation is resonant and its amplitude can therefore vary by several orders of magnitude as a function of the tidal frequency (Ogilvie & Lin, 2004; Auclair-Desrotour, Mathis & Le Poncin-Lafitte, 2015), particularly in the case of weak effective turbulent viscosity expected in the case of rapidly rotating planets (Mathis, 2016). Hence, it can explain the increase by one order of magnitude of the dissipation over the small frequency range arising between Dione and Rhea. Fuller et al. (2016) also proposed an alternative scenario by studying gravito-inertial waves (their restoring forces are the Coriolis acceleration and the Archimedean buoyancy force) that propagate and are trapped in resonance in a potential stably-stratified layer surrounding the core (Fuller et al. 2014).

5. Discussion

In 1977, Gavrilov and Zharkov (1977) computed the value of Saturn's Love numbers and obtained for the lowest degree quadrupolar coefficient $k_2=0.341$. Even though this value is often used as the reference, it stands on physical assumptions and internal structure models that have since been improved (Guillot 1999, 2005; Hubbard et al., 2009; Kramm et al., 2011; Nettelmann et al., 2013; Helled & Guillot, 2013). Although all the models we consid-

ered following the approach of Helled and Guillot (2013) reproduced the gravitational coefficients J_2 , J_4 and J_6 with error bars, they lead to significant variations in k_2 . J_2 and k_2 are both sensitive to the density profile, but in a different manner. For slowly rotating bodies, J_2 and fluid Love number k_2^f (which is very close to the tidal Love number in the case of Saturn) can be related through the classical relationship $J_2=qk_2^f/3$ with q the rotational parameter: $q=\omega^2 a^3/GM$, with ω the rotation frequency, a the equatorial radius, M the mass of the planet and G the gravitational constant. For Saturn, the rotational ratio q ranges between 0.1544 and 0.1584 for rotation periods between 10h32' and 10h39'. Such a high q ratio, the fluid Love number predicted from the simple J_2 relationship is about 0.31, which is about 13–18% less than the fluid Love number computed from the density profile. This is due to the strong flattening of the planet and the gravitational signatures of the flattened internal interfaces. As already anticipated from the pioneer work of Gavrilov and Zharkov (1977) and further explored by Kramm et al. (2011), the Love number k_2 is very sensitive to the degree of mass concentration toward the center of the planet, but differently from J_2 . It evaluates the amplitude of the hydrostatic adjustment of the planet's structure to the tidal perturbations while J_2 gives the strength of the hydrostatic response to the centrifugal acceleration. Determinations of the tidal Love numbers (k_2 , k_3) and of the gravitational coefficients thus provide complementary information to constrain the density structure of Saturn. From the variety of internal models we explored in the present study, we notice that a large fraction of models compatible with

the J_n coefficients are compatible with the inferred k_2 because the uncertainties are still large. However, any further improvement in the estimation of k_2 and the spin rate will allow to restrict the number of acceptable models and provide crucial constraints on Saturn's interior.

Our estimation of Saturn's Q confirms the values previously derived by Lainey et al. (2012), which is one order of magnitude smaller than the value derived from the usually expected long term evolution of the Moons over the age of the Solar System (Sinclair, 1983). We recall that earlier studies constrained Saturn's Q using the current positions of the innermost main Moons. Considering the Moons' motions back in time, the averaged exchange of angular momentum between the planet and the Moons associated with tidal dissipation must have been limited in order to prevent the Moons from crossing their Roche limit 4.5 Byr ago (Goldreich & Soter 1966). Such a Q value was then re-evaluated by Gavrilov & Zharkov (1977) using a more realistic k_2 for Saturn and by Sinclair (1983) considering in detail the Mimas-Tethys 2:1 mean motion resonance. The low Q or high dissipation rate obtained in this work, implying rapid orbital expansion, suggests that either the dissipation has significantly changed over time, or that the Moons formed later after the formation of the Solar System (Charnoz et al. 2011; Ćuk 2014). Since tidal dissipation may arise both in the planet's fluid envelope and its presumably solid core (Guenel et al., 2014), we can look in more detail at the frequency dependency of the tidal ratio k_2/Q shown in Fig. 1. Despite large error bars, the tidal ratios associated with Enceladus, Tethys and Dione do not depart from their former constant estimates. On the other hand, we obtain a strong increase of dissipation at Rhea's frequency. Such a dissipation corresponds to an orbital shift in the longitude of about 75 km (see Appendix A.3). The fact that the strong orbital shift at Rhea is observed using both the IMCCE and JPL models, makes systematic errors unlikely. As Rhea has no orbital resonance with any other Moon, and no significant dynamical interaction with the rings, its strong orbital shift is more likely the consequence of strong tides.

The rather constant dissipation inferred at tidal frequencies associated with Enceladus, Tethys and Dione suggests dissipation processes dominated by anelastic tidal friction in a solid core (Remus et al., 2012, 2015). This is confirmed by the calculations performed here using more realistic density profiles. We further show that a Q factor lower than 3000 required a core viscosity lower than 10^{16} Pa.s. For large low-density ice-rich cores, Q values as low as 200–300, compatible with the k_2/Q estimate obtained at Rhea's frequency, can be obtained. However, due to the weak frequency dependence of dissipation in a viscoelastic core, a Q value of 1500–2500 at Enceladus, Tethys and Dione's frequency cannot be match simultaneously with a value as low as 300 at Rhea's. This suggests either that additional dissipation processes exist in Saturn at Rhea's frequency to reduce the apparent Q value, or that a value as low as 300 is representative of Saturn's dissipation that the orbital consequences of such a strong dissipation in Saturn is partially compensated by strong dissipation in the Moons. The best candidate for additional processes in Saturn to explain the reduced Q at Rhea's is friction applied to tidal inertial (or gravito-inertial) waves in the deep, rapidly rotating, gaseous envelope of Saturn that dissipates their kinetic energy (Ogilvie & Lin, 2004; Fuller et al., 2016). It can explain the increase by one order of magnitude of the dissipation over the small frequency range arising between Dione and Rhea.

6. Conclusion

Using a large set of astrometric observations including ground-based observations and thousands of Cassini-ISS data, we provide the first observationally-derived estimate of the Love number of

Saturn, k_2 . This determination could be done thanks to the presence of the lagrangian Moons of Tethys and Dione in the dynamical modeling. Moreover, we confirm the strong tidal dissipation found by Lainey et al. (2012), but associated with an intense frequency-dependent peak of tidal dissipation for Rhea's tidal frequency. Modeling the likely interior of Saturn, it appears two different tidal mechanisms may arise simultaneously within the planet. The first one is tidal friction within the dense core, while significant tidal dissipation may also occur inside the outer fluid envelope at Rhea's tidal frequency.

Note added in proof

Wahl et al. (2016) recently presented theoretical calculations for one symmetrically spherical Saturn model yielding a value of $k_2=0.367$, in agreement with the theoretical static values presented in Section 4. However, they show that accounting for dynamical flattening due to rotation increases the total theoretical k_2 value by +0.046. This is still compatible with our constraint $k_2=0.390 \pm 0.024$ but would imply that our analysis in Fig. 2 should be reconsidered.

Acknowledgments

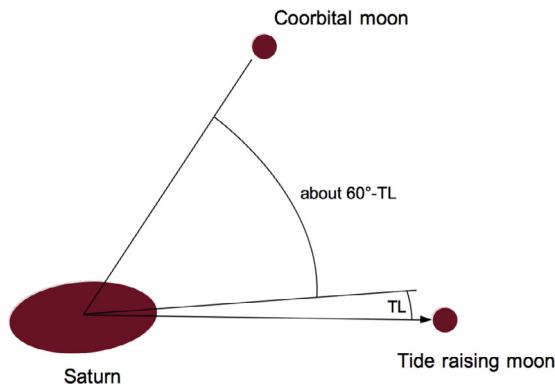
The authors are indebted to all participants of the Encelade WG. V.L. would like to thank Michael Efroimsky for fruitful discussions. This work has been supported by the European Community's Seventh Framework Program (FP7/2007-2013) under grant agreement 263466 for the FP7-ESPaCE project, the International Space Science Institute (ISSI), PNP (INSU/CNES) and AS GRAM (INSU/CNES/INP). The work of R. A. J. was carried out at the Jet Propulsion Laboratory, California Institute of Technology, under a contract with NASA. N.C. and C.M. were supported by the UK Science and Technology Facilities Council (Grant No. ST/M001202/1) and are grateful to them for financial assistance. C.M. is also grateful to the Leverhulme Trust for the award of a Research Fellowship. N.C. thanks the Scientific Council of the Paris Observatory for funding. S. Mathis acknowledges funding by the European Research Council through ERC grant SPIRE 647383. G. Tobie acknowledges funding from the European Research Council under the European Community's Seventh Framework Programme (FP7/2007-2013 Grant Agreement no. 259285, ERC EXOATER). The authors are indebted to the Cassini project and the Imaging Science Subsystem Team for making this collaboration possible.

Appendix

A.1. The tidal effects on coorbital satellites

The effects of tidal bulges on one Moon's motion are generally far below detection, unless those tides are raised by the same Moon. Indeed, such a configuration produces a secular effect on the orbit that may be detectable after a sufficient amount of time. On the other hand, tidal bulges associated with another Moon will introduce essentially quasi-periodic perturbations, with much lower associated signal on the orbits. There exists an exception, however, if one considers the special case of lagrangian Moons. Indeed, in such a case the tidal bulges are oriented on average with a constant angle close to 60° (see figure below).

As a consequence, tidal effects arising on one Moon and acting on a lagrangian Moon will provide a significant secular signature on the orbital longitude that is hopefully detectable. To quantify how large this effect can be, we rely here on numerical simulation. A simple look at the differences on the positions of the coorbital Moons after adding/removing the cross tidal effects over about 10 years (roughly the time span of Cassini data) will be meaningless.



Indeed, one needs to take into account the fitting procedure of the initial conditions to the observations. In particular, the difference in modeling may be partly masked by a slight change of the initial conditions. As a consequence, the true incompressible part of the cross tidal effects in the dynamics will be revealed only after having fitted one simulation onto the other. We provide below pre-fit and postfit residuals associated with these cross-tidal effects, for 14 Moons of Saturn. The postfit simulations are obtained after having fitted all initial state vectors, masses, Saturn’s J_2 , polar orientation and precession, Saturn’s tidal Q .

We can see that the largest effects indeed appear on the coorbital Moons, with the highest effects on the lagrangian satellites of Tethys and Dione. When not considering these cross-tidal effects, the astrometric residuals of these former Moons can easily reach a few tens of kilometers, much above the typical 5 km residuals we obtained in the present work (see Appendix A.4 and Fig. A.4).

A.2. Validation of Love number computation

A.3. Rhea’s orbital acceleration under strong Saturnian tides

To estimate the impact of the large k_2/Q value obtained at Rhea’s tidal frequency, we perform prefit and postfit simulations (fitting the state vectors of all Moons) over a century. Assuming $k_2/Q=122.28 \times 10^{-5}$ (see IMCCE solution in Table 1), the postfit residuals below show that Rhea’s longitude is affected by a signal of a bit more than 75 km. This corresponds to about 12.5 mas (0.0125 arc second) at opposition, which represents roughly 10% of the global astrometric residuals from the ground (Lainey et al. 2012), and a huge signal when comparing with Cassini data.

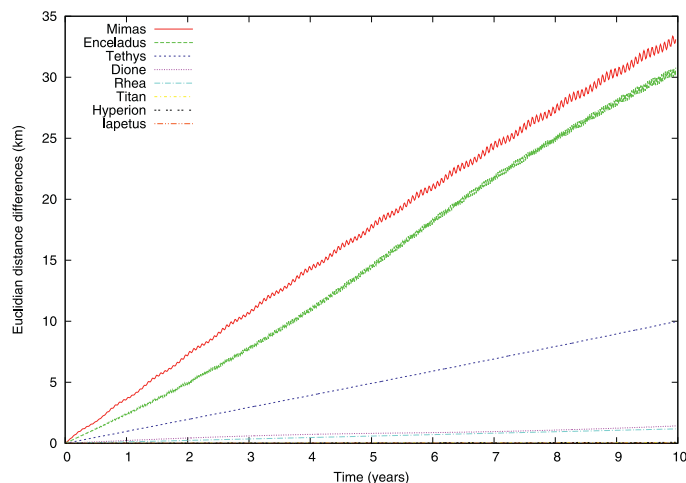


Table A.4.1
(One single Moon per image): Statistics of the ISS-NAC astrometric residuals computed from IMCCE model (no tidal dissipation within Enceladus scenario) in pixel. μ and σ denote respectively the mean and standard deviation of the residuals computed on sample and line. N_s and N_l are the number of observations considered for the respective coordinate.

Satellite	μ_s	σ_s	μ_l	σ_l	N_s	N_l
Epimetheus	-0.0094	4.3180	0.1805	4.5340	350	350
Janus	0.0096	0.9780	0.5378	1.1566	322	322
Mimas	0.4190	0.2813	-0.0460	0.6600	20	20
Enceladus	-0.0014	0.3547	-0.1116	0.2783	108	108
Tethys	-0.1232	0.5284	0.0814	0.2600	25	25
Dione	-0.0278	0.4808	0.0748	0.4730	84	84
Rhea	-0.2925	0.4644	-0.0035	0.2055	58	58
Titan	0.0000	0.0000	0.0000	0.0000	0	0
Hyperion	0.0000	0.0000	0.0000	0.0000	0	0
Iapetus	0.0000	0.0000	0.0000	0.0000	0	0
Calypso	-0.0348	0.2508	-0.1742	0.2546	230	230
Telesto	-0.0190	0.2220	-0.0366	0.2960	279	279
Helene	-0.0164	0.2731	-0.0456	0.2492	262	262
Polydeuces	-0.0554	0.2508	-0.0584	0.2422	139	139

Table A.4.2
(Multiple Moon per image): Statistics of the ISS-NAC astrometric residuals computed from IMCCE model (no tidal dissipation within Enceladus scenario) in pixel. μ and σ denote respectively the mean and standard deviation of the residuals computed on sample and line. N_s and N_l are the number of observations considered for the respective coordinate.

Satellite	μ_s	σ_s	μ_l	σ_l	N_s	N_l
Epimetheus	0.0203	0.2778	0.0449	0.2912	28	28
Janus	-0.0203	0.2778	-0.0449	0.2912	28	28
Mimas	0.0255	0.1784	-0.0064	0.2745	134	134
Enceladus	-0.0307	0.1784	0.0084	0.1248	327	327
Tethys	0.0211	0.1088	0.0186	0.1359	424	424
Dione	-0.0204	0.1061	0.0054	0.1070	592	592
Rhea	0.0175	0.1370	-0.0234	0.1208	556	556
Titan	0.0000	0.0000	0.0000	0.0000	0	0
Hyperion	0.0000	0.0000	0.0000	0.0000	0	0
Iapetus	0.0000	0.0000	0.0000	0.0000	0	0
Calypso	0.1470	0.0000	-0.5137	0.0000	1	1
Telesto	-0.0997	0.0702	0.2454	0.1691	3	3
Helene	-0.1308	0.0508	0.2090	0.0096	2	2
Polydeuces	0.1379	0.0731	-0.2135	0.1657	3	3

A.4. Astrometric residuals and linear correlations

To illustrate the various simulations that we performed, we provide astrometric residuals of the IMCCE solution that considered a

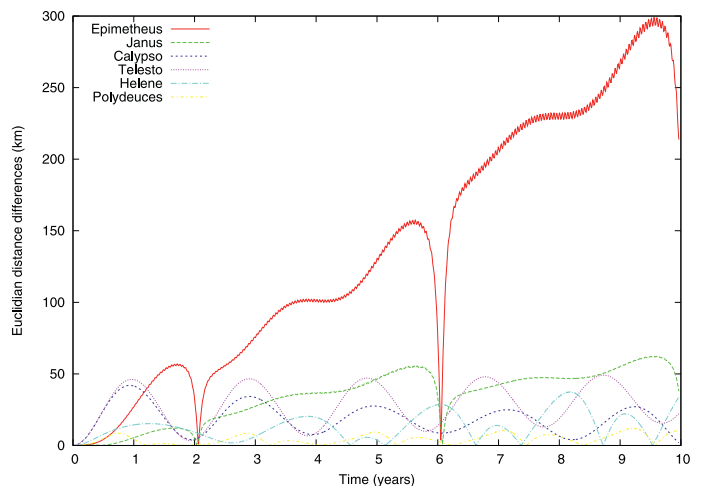


Fig. A.1.1. Prefit residuals associated with cross-tidal effects.

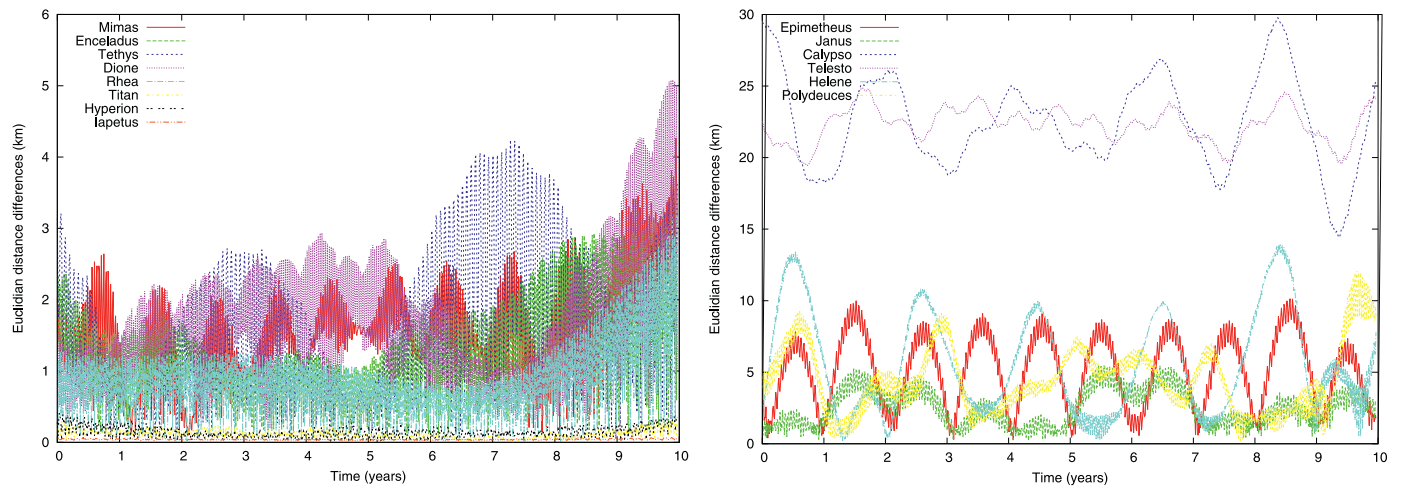


Fig. A.1.2. Postfit residuals associated with cross-tidal effects.

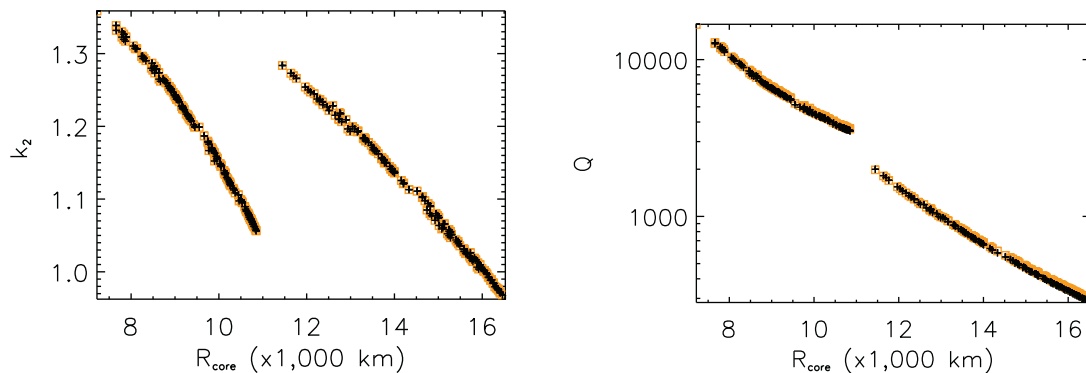


Fig. A.2. Comparison between numerical (black crosses) and analytical (orange squares) solutions of tidal Love number, k_2 (left) and dissipation factor, Q (right) as a function of core radius, R_{core} , computed for a solid viscoelastic core and a fluid envelope with constant density, assuming a core viscosity of 10^{15} Pa.s and a shear modulus of 1000 GPa.

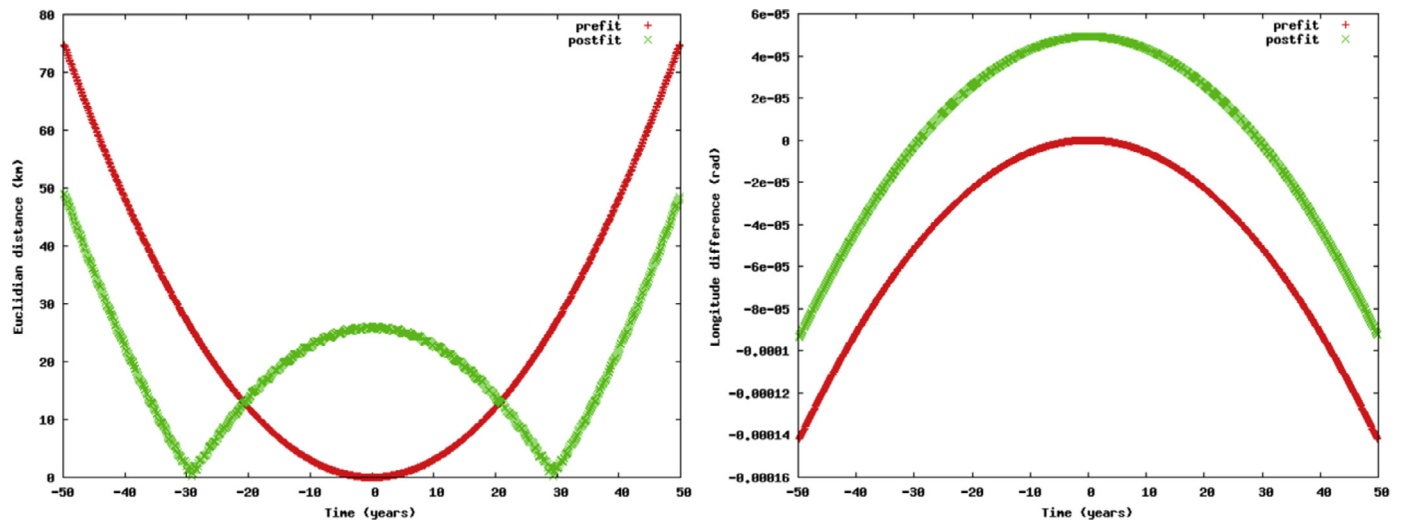


Fig. A.3.1. Left: residuals in distance (km); right: residuals in the orbital longitude (rad).

constant k_2/Q ratio and no tidal dissipation scenario within Enceladus. To save space, we do not provide here statistics of ground-based and HST data, since they are pretty similar to the ones published in Lainey et al. (2012). We provide below the plots of the O-Cs, only. Full statistics are available on request.

Fig. A.4 shows the astrometric residuals of the lagrangian satellites of Tethys and Dione. Tables A.4.1–A.4.3 provide the astrometric residuals of all observations for the 14 Moons considered. Table A.4.4 provides the correlations between all our fitted parameters and the tidal parameters k_2 and Q .

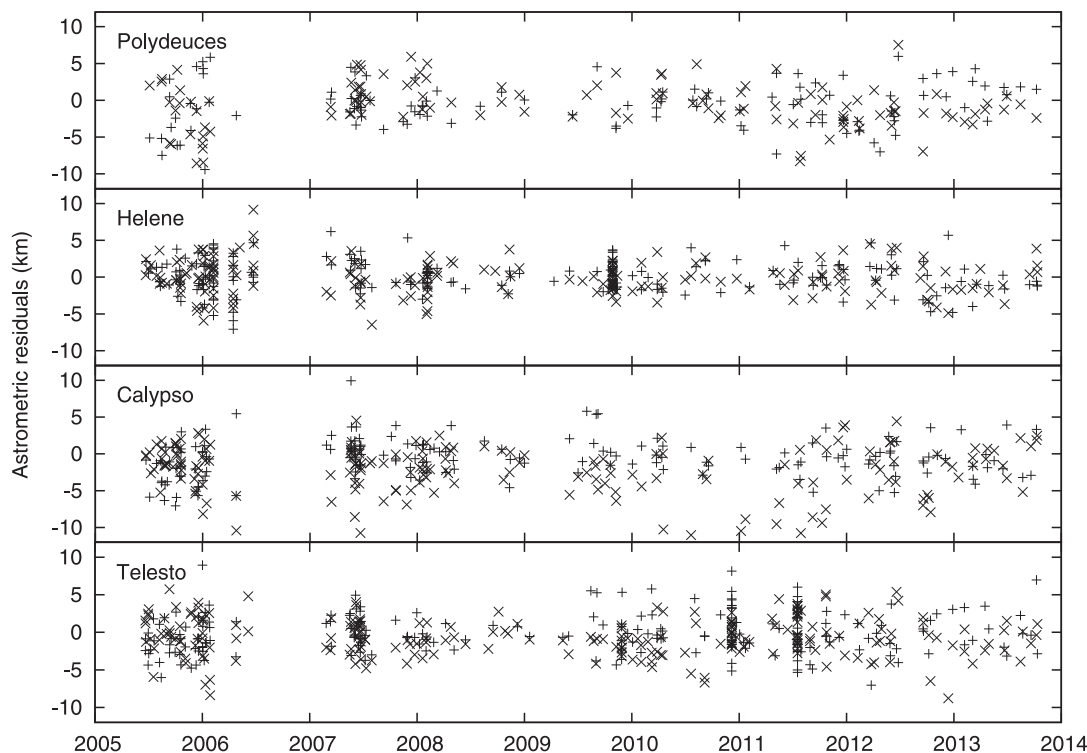


Fig. A.4.1. Astrometric residuals of the four lagrangian satellites from ISS-Cassini. Telesto and Calypso are the two coorbital Moons of Tethys. They move around the lagrangian stable points L4 and L5. Helene and Polydeuces are in equivalent orbital configurations but along the orbit of Dione. The associated ISS-NAC astrometric data are fitted in sample and line coordinates (pixel). Residuals are here converted to kilometres.

Table A.4.3

(One Moon per image): Statistics of the ISS-NAC astrometric residuals computed from IMCCE model (no tidal dissipation within Enceladus scenario) in km. μ and σ denote respectively the mean and standard deviation of the residuals computed on RA and DEC. N_{RA} and N_{DEC} are the number of observations considered for the respective coordinate.

Satellite	μ_{RA}	σ_{RA}	μ_{DEC}	σ_{DEC}	N_{RA}	N_{DEC}
Mimas	-1.1001	3.9151	-1.1401	2.8370	826	826
Enceladus	-0.1979	2.8234	0.2713	2.6588	732	732
Tethys	0.0532	4.5654	-0.0123	3.5007	924	924
Dione	-0.2068	4.1726	-0.5264	3.4948	948	949
Rhea	-0.3170	3.3581	-0.1138	2.4739	1021	1021
Titan	0.0000	0.0000	0.0000	0.0000	0	0
Hyperion	-0.1292	15.4526	-5.9373	12.7287	92	90
Iapetus	1.4754	5.1951	-1.1544	5.4322	1534	1534

Table A.4.4 (continued)

	k_2	Q
l_3	-0.013	0.232
k_3	-0.013	0.017
h_3	-0.003	0.002
q_3	0.017	-0.024
p_3	0.002	0.070
a_4	0.009	0.027
l_4	-0.012	0.182
k_4	0.017	0.084
h_4	-0.026	-0.026
q_4	0.004	-0.000
p_4	-0.006	0.127
a_5	0.009	0.024
l_5	0.009	-0.223
k_5	0.000	0.020
h_5	-0.003	-0.074
q_5	-0.027	0.012
p_5	0.011	0.069
a_6	0.009	0.026
l_6	0.002	-0.509
k_6	0.011	-0.005
h_6	-0.010	0.082
q_6	0.005	-0.012
p_6	-0.007	0.154
a_7	0.009	0.023
l_7	-0.003	-0.216
k_7	-0.006	-0.029
h_7	-0.003	-0.008
q_7	-0.006	0.203
p_7	-0.007	0.036
a_8	0.010	0.019
l_8	-0.002	-0.005
k_8	-0.002	-0.003
h_8	0.003	0.025
q_8	0.006	0.059
p_8	0.002	-0.013
a_9	0.007	0.016
l_9	-0.001	-0.005

Table A.4.4

Correlation between all our fitted parameters and the tidal parameters k_2 and Q . Here a is the semi-major axis, l is the mean longitude, e is the eccentricity, Ω is the longitude of the node, ω is the argument of the periapsis, $k=e \cos(\Omega+\omega)$, $h=e \sin(\Omega+\omega)$, $q=\sin(i/2) \cos(\Omega)$ and $p=\sin(i/2) \sin(\Omega)$. Numbers 1,2,3,...,14 refer to Epimetheus, Janus, the eight main Moons (Mimas,...Iapetus), Calypso, Telesto, Helene, Polydeuces, respectively. Full table is available on request.

	k_2	Q
a_1	0.006	0.023
l_1	0.002	-0.014
k_1	-0.000	-0.001
h_1	0.002	0.002
q_1	-0.000	-0.002
p_1	0.000	0.003
a_2	0.008	0.025
l_2	-0.004	-0.029
k_2	-0.001	0.002
h_2	-0.002	0.001
q_2	0.000	-0.001
p_2	-0.000	0.002
a_3	0.009	0.025

Table A.4.4 (continued)

	k_2	Q
k_9	-0.001	0.001
h_9	0.002	0.014
q_9	-0.003	-0.000
p_9	0.000	-0.018
a_{10}	0.008	0.008
l_{10}	-0.004	-0.007
k_{10}	-0.008	-0.005
h_{10}	-0.007	-0.007
q_{10}	0.000	0.005
p_{10}	-0.002	-0.022
a_{11}	0.010	0.025
l_{11}	-0.024	-0.114
k_{11}	0.034	0.003
h_{11}	-0.012	-0.002
q_{11}	-0.028	0.029
p_{11}	0.018	0.051
a_{12}	0.008	0.025
l_{12}	0.142	-0.216
k_{12}	-0.002	-0.011
h_{12}	-0.012	-0.006
q_{12}	0.025	-0.018
p_{12}	0.011	0.026
a_{13}	0.005	0.025
l_{13}	-0.028	-0.254
k_{13}	0.010	0.033
h_{13}	-0.002	0.026
q_{13}	-0.000	-0.031
p_{13}	0.001	0.062
a_{14}	0.010	0.029
l_{14}	-0.073	-0.254
k_{14}	0.020	-0.055
h_{14}	0.007	-0.052
q_{14}	0.004	-0.021
p_{14}	-0.005	0.054
M	0.009	0.026
m_1	-0.004	0.003
m_2	-0.004	0.003
m_3	-0.001	-0.378
m_4	0.038	-0.064
m_5	0.118	-0.019
m_6	0.120	0.029
m_7	0.011	-0.062
m_8	0.000	0.004
m_9	0.000	-0.003
m_{10}	-0.005	-0.011
a_0	0.003	-0.591
d_0	-0.010	0.138
c_{20}	-0.005	0.014
da/dt	0.017	0.186
dd/dt	0.012	-0.129
k_2	1.000	-0.030
Q	-0.030	1.000

References

- Alterman, Z., Jarosch, H., Pekeris, C.L. 1959, Proceedings of the Royal Society of London Series A, 252, 80.
- Auclair-Desrotour, P., Mathis, S., Le Poncin-Lafitte, C., 2015. Scaling laws to understand tidal dissipation in fluid planetary regions and stars I. Rotation, stratification and thermal diffusivity. *A&A* 581, A118.
- Braviner, H.J., Ogilvie, G.I., 2015. Tidal interactions of a Maclaurin spheroid. II: Resonant excitation of modes by a close, misaligned orbit. *Mon. Not. R. Astron. Soc.* 447, 1145–1157.
- Charnoz, S., et al., 2011. Accretion of Saturn's mid-sized Moons during the viscous spreading of young massive rings: Solving the paradox of silicate-poor rings versus silicate-rich Moons. *Icarus* 216, 535.
- Cooper, N.J., et al., 2014. Cassini ISS mutual event astrometry of the mid-sized Saturnian satellites 2005–2012. *Astron. Astrophys.* 572, 8.
- Ćuk, M. Recent Origin of Titan's Orbital Eccentricity. American Astronomical Society, DDA meeting #45, #301.01 (2014).
- Dermott, S.F., 1979. Tidal dissipation in the solid core of major planets. *Icarus* 37, 310.
- Desmars, J., Vienne, A., Arlot, J.E., 2009. A new catalogue of observations of the eight major satellites of Saturn (1874–2007). *Astron. Astrophys.* 493, 1183.
- Dziewonski, A.M., Anderson, D.L. 1981, Physics of the Earth and Planetary Interiors, 25, 297.
- Fuller, J., Luan, J., Quataert, E., 2016. Resonance locking as the source of rapid tidal migration in the Jupiter and Saturn systems. *MNRAS* 458, 3867.
- Fuller, J., 2014. Saturn ring seismology: Evidence for stable stratification in the deep interior of Saturn. *Icarus* 242, 283–296.
- Gavrilov, S.V., Zharkov, V.N., 1977. Love numbers of the giant planets. *Icarus* 32, 443–449.
- Goldreich, P., Soter, S., 1966. Q in the Solar System. *Icarus* 5, 375–389.
- Guenel, M., Mathis, S., Remus, F., 2014. Unravelling tidal dissipation in gaseous giant planets. *Astron. Astrophys.* 566, L9.
- Guillot, T., 1999. Interior of giant planets inside and outside the Solar System. *Science* 286, 72–77.
- Guillot, T., 2005. The interiors of giant planets: Models and outstanding questions. *Annual Rev. Earth Planet. Sci.* 33, 493–530.
- Helled, R., Galanti, E., 2015. Kaspi, Yohai Saturn's fast spin determined from its gravitational field and oblateness. *Nature* 520, 202.
- Helled, R., Guillot, T., 2013. Interior models of Saturn: including the uncertainties in shape and rotation. *Astrophys. J.* 767, 113.
- Hubbard, W.B., Dougherty, M.K., Gautier, D., et al. The Interior of Saturn. In: Dougherty, M. K., Esposito, L. W., Krimigis, S. M., Saturn from Cassini-Huygens. ISBN 978-1-4020-9216-9. Springer Science+Business Media B.V., 2009, p. 75 (2009).
- Jacobson, R.A., Antreasian, P.G., Bordi, J.J., et al., 2006. The gravity field of the saturnian system from satellite observations and spacecraft tracking data. *The Astron. J.* 132, 2520–2526.
- Jacobson, R.A., et al., 2006. The gravity field of the Saturnian system from satellite observations and spacecraft tracking data. *Astron. J.* 132, 2520.
- Kaula, W.M., 1964. Tidal dissipation by solid friction and the resulting orbital evolution. *Rev. Geophys. Space Phys.* 2, 661.
- Karato, S.-i. 2008, Physics of the Earth and Planetary Interiors, 170, 152.
- Kramm, U., Nettelmann, N., Redmer, R., et al., 2011. On the degeneracy of the tidal Love number k_2 in multi-layer planetary models: application to Saturn and GJ 436b. *Astron. Astrophys.* 528, A18.
- Lainey, V., Dehant, V., Pätzold, M., 2007. First numerical ephemerides of the martian Moons. *Astron. Astrophys.* 465, 1075–1084.
- Lainey, V., Arlot, J.E., Karatekin, Ö., et al., 2009. Strong tidal dissipation in Io and Jupiter from astrometric observations. *Nature* 459, 957–959.
- Lainey, V., et al., 2012. Strong tidal dissipation in Saturn and Constraints on Enceladus' thermal state from astrometry. *Astrophys. J.* 752, 14.
- Lainey, V., 2008. A new dynamical model for the uranian satellites. *Planet. Space Sci.* 56, 1766–1772.
- Mathis, S., Auclair-Desrotour, P., Guenel, M., et al., 2016. The impact of rotation on turbulent tidal friction in stellar and planetary convective regions. *A&A* 592, A33.
- Meyer, J., Wisdom, J., 2007. Tidal heating in Enceladus. *Icarus* 188, 535–539.
- Morales, M.A., et al., 2009. Phase separation in hydrogen-helium mixtures at Mbar pressures. *Proc. Nat. Acad. Sci.* 106, 1324–1329.
- Moyer, T.D., 2000. Formulation for observed and computed values of Deep Space Network data types for navigation. In: Deep Space Communications and Navigation Series: Monograph 2. Jet Propulsion Laboratory, Pasadena, CA.
- Nettelmann, N., Püstow, R., Redmer, R., 2013. Saturn layered structure and homogeneous evolution models with different EOSs. *Icarus* 225, 548.
- Newhall, X.X., Standish, E.M., Williams, J.G., 1983. DE 102 - A numerically integrated ephemeris of the Moon and planets spanning forty-four centuries. *Astron. Astrophys.* 125, 150–167.
- Ogilvie, G.I., Lin, D.N.C., 2004. Tidal dissipation in rotating giant planets. *Astrophys. J.* 610, 477–509.
- Peters, C.F., 1981. Numerical integration of the satellites of the outer planets. *Astron. Astrophys.* 104, 37.
- Remus, F., Mathis, S., Zahn, J.-P., et al., 2012. Anelastic tidal dissipation in multi-layer planets. *Astron. Astrophys.* 541, 165.
- Remus, F., Mathis, S., Zahn, J.-P., et al., 2015. The surface signature of the tidal dissipation of the core in a two-layer planet. *Astron. Astrophys.* 573, 23.
- Robert, V., et al., 2011. A new astrometric reduction of photographic plates using the DAMIAN digitizer: Improving the dynamics of the jovian system. *Mon. Not. R. Astron. Soc.* 415, 701.
- Robert, V. et al., A new astrometric measurement and reduction of USNO photographic observations of the main Saturnian satellites 1974–1998. *A&A* (2016) to be submitted.
- Saito, M., 1974. Some problems of static deformation of the Earth. *J. Phys. Earth* 22, 123.
- Sinclair, A.T., 1983. A re-consideration of the evolution hypothesis of the origin of the resonances among Saturn's satellites. In: Dynamical trapping and evolution in the Solar System; Proceedings of the Seventy-fourth Colloquium, Gerakini, Greece, August 30–September 2, 1982 (A84-34976 16-89). D. Reidel Publishing Co., Dordrecht, pp. 19–25.
- Tajeddine, R., Cooper, N.J., Lainey, V., et al., 2013. Astrometric reduction of Cassini ISS images of the Saturnian satellites Mimas and Enceladus. *Astron. Astrophys.* 551, 129.
- Tajeddine, R., Lainey, V., Cooper, N.J., et al., 2015. Cassini ISS astrometry of the Saturnian satellites: Tethys, Dione, Rhea, Iapetus, and Phoebe 2004–2012. *Astron. Astrophys.* 575, A73.
- Takeuchi, H., Saito, M., 1972. Seismic surface waves. *Meth. Comput. Phys.* 11, 217–295.
- Tobie, G., Mocquet, A., Sotin, C., 2005. Tidal dissipation within large icy satellites: Applications to Europa and Titan. *Icarus* 177, 534.